



HAL
open science

Calibration methods and uncertainties estimation of WEST infrared thermography diagnostics

X. Courtois, Mh. Aumeunier, L. Dubus, J. Gaspar, M. Houry, R. Mitteau

► **To cite this version:**

X. Courtois, Mh. Aumeunier, L. Dubus, J. Gaspar, M. Houry, et al.. Calibration methods and uncertainties estimation of WEST infrared thermography diagnostics. *Fusion Engineering and Design*, 2023, 190, pp.113506. 10.1016/j.fusengdes.2023.113506 . hal-04302195

HAL Id: hal-04302195

<https://hal.science/hal-04302195>

Submitted on 23 Nov 2023

HAL is a multi-disciplinary open access archive for the deposit and dissemination of scientific research documents, whether they are published or not. The documents may come from teaching and research institutions in France or abroad, or from public or private research centers.

L'archive ouverte pluridisciplinaire **HAL**, est destinée au dépôt et à la diffusion de documents scientifiques de niveau recherche, publiés ou non, émanant des établissements d'enseignement et de recherche français ou étrangers, des laboratoires publics ou privés.

Calibration methods and uncertainties estimation of WEST infrared thermography diagnostics

X. Courtois^a, MH. Aumeunier^a, L. Dubus^a, J. Gaspar^b, M. Houry^a, R. Mitteau^a

^a CEA-IRFM, F-13108 Saint-Paul-Lez-Durance, France

^b Aix-Marseille Univ., CNRS, IUSTI, Marseille, France

Abstract. . This paper presents the method toward quantifying the global uncertainty on the blackbody temperature measurement from the infrared (IR) diagnostics of WEST. To address this goal, the main functional elements of the IR diagnostics are identified. Then the temperature calibration and calculation principles are presented and analysed to extract the main potential uncertainty contributors, such as the optical transmission coefficients and their stray lights, or the accuracy of temperature references used for calibration. These contributors are individually estimated, or experimentally measured when a supposed effect on the overall uncertainty is identified, like environmental conditions or parasitic radiations. In particular, effects of environmental temperature on the transmission lines and camera is thoroughly studied. All contributions are then aggregated in the uncertainty propagation calculation and results in an overall temperature uncertainty versus the temperature estimation. The uncertainty is in the range of 5-10% for blackbody temperatures above 200°C, and progressively worsens when temperature decreases.

1 Introduction

The WEST tokamak is equipped with a set of infrared (IR) diagnostics, composed of twelve IR cameras (2022 configuration), which measure the IR radiation emitted by the in-vessel components: heating antennas, divertors, bumpers, baffles, etc. Figure 1 shows the spatial covering of the IR views. The radiance collected by camera (in $\text{W}\cdot\text{m}^{-2}\cdot\text{sr}^{-1}$) is converted in blackbody surface temperature, which is an indispensable information for the components monitoring (real time processing) to prevent excessive heating, as well as to offer essential data for many physics studies (post processing) [1].

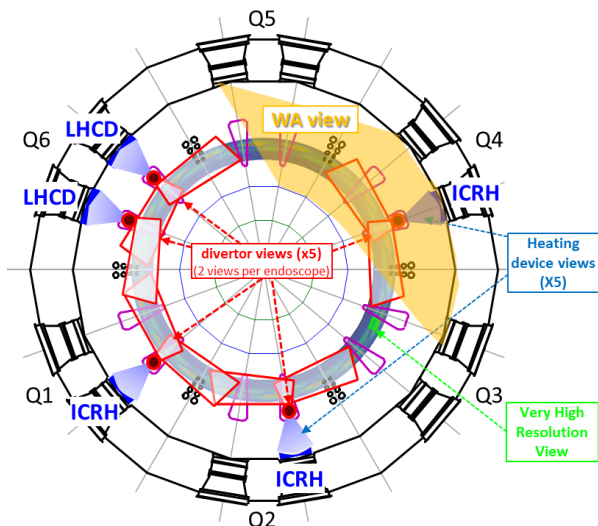


Figure 1 : scheme of the IR diagnostics views spatial covering, from above

WEST IR diagnostics mainly consists of a set of 5 endoscopes, as described in [2-3], located in the upper ports of the machine and viewing downward, each one being equipped by 2 IR cameras: one for a divertor view and one on a heating device (ICRH or LHCD). These upper ports endoscopes were developed for the former Tore Supra Configuration (2005) and refurbished for WEST in 2015. This set is completed by 2 distinctive views developed for WEST: a wide angle (WA) tangential view [2, 4] located in an equatorial port, and a very high-resolution (VHR) view [2, 5] focused on the divertor with a 0.1 mm pixel resolution. Their optical designs differ, but all views are equipped by the same IR cameras, and share the same data acquisition and real-time processing unit, as well as the same temperature calculation algorithms.

2 Temperature calculation and calibration methods

Since calibration in laboratory cannot reproduce tokamak temperature environment (unless with a complex test bed device), it is necessary to take into account the temperature difference between laboratory and tokamak environment in the calibration process. That implies to decompose the optical system into independent parts, and to characterise them separately. The basis of the method is used for long time at IRFM for the upper ports endoscopes [6], and has been modified for its adaptation to the new WEST diagnostics.

The optical path of each endoscope is split into sub-systems that are considered isothermal. A maximum of

3 optical sub-system is used for simplification, however, the method is applicable for any number. These sub-systems differ for each kind of diagnostic mentioned in §1 and are resumed in the table 1. An optical sub-system can be composed of one or several lenses, window or mirror, the main point being that its temperature is known, and is considered isothermal and almost constant during pulses, which is quite true since almost all optical components are cooled when located in-vessel or are in atmosphere.

Table 1: decomposition of IR diagnostic into optical sub-systems, and their temperature (Hot loop=vacuum vessel cooling loop temperature usually 70°C, Cold loop=cold cooling loop temperature usually 20°C) and transmission coefficient τ (or reflection coefficient for mirrors)

Diag.	Optic 1 Temperature & Transmission	Optic 2 Temperature & Transmission	Optic 3 Temperature & Transmission
Div view	2 sapphire windows (head entrance pupil) $T=Hot\ loop$ $\tau=0.76$	4 relay lenses + outlet sapphire window $T=Cold\ loop.$ $\tau=0.2$	Not used $\tau=1$
Ant view	1 deflecting mirror $T=Hot\ loop$ $\tau=0.9$	2 sapphire windows (head entrance pupil) $T=Hot\ loop$ $\tau=0.76$	4 relay lenses + outlet sapphire window $T=Cold\ loop.$ $\tau=0.07$
VHR view	2 head mirrors $T=Hot\ loop$ $\tau=0.8$	2 relay mirrors $T=Hot\ loop$ $\tau=0.8$	sapphire window + 2 relays mirrors $T=Atm. + 20^\circ C$ $\tau=0.64$
WA view	2 head mirrors $T=Hot\ loop$ $\tau=0.8$	outlet sapphire window $T=Atmosph. + 20^\circ C$ $\tau=0.8$	Not used $\tau=1$

Based on this decomposition, the scheme in the Figure 2 describes the radiation propagation along the optical system. At each optical sub-system step i , the incoming radiance is reduced by the transmission coefficient τ_i and the parasitic radiance (straylight) emitted by the optical components of the sub-system $(1-\tau_i).R(T_i)$ is added.

In this study, the radiance reflected on lenses is neglected since all optical surfaces are anti-reflection coated. Diffuse reflection on mirrors and parasitic radiance emitted by internal surfaces of optical systems are also considered insignificant and are then neglected in the straylight formulation.

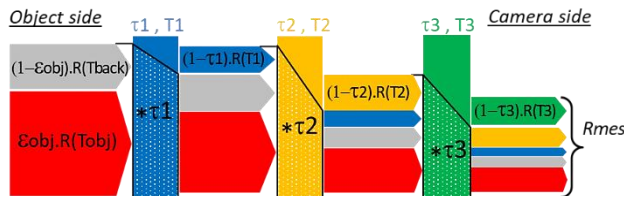


Figure 2 : radiation propagation scheme from the thermal scene (object side) to the camera through the optical path composed of 3 optical sub-systems.

Thus, the measured radiance R_{mes} can be written:

$$R_{mes} = ((Remit)\tau_1 + (1-\tau_1)R(T_1))\tau_2 + (1-\tau_2)R(T_2)\tau_3 + (1-\tau_3)R(T_3) \quad (1)$$

R_{mes} : radiance measured by the camera

$R(T_i)$ = radiance emitted by the sub-system i at temp. T_i .

$Remit$: radiance emitted by the thermal scene:

$$Remit = \epsilon_{obj}.R(T_{obj}) + (1-\epsilon_{obj})R(T_{back}) \quad (2)$$

T_{obj} = object temperature

ϵ_{obj} = object emissivity

T_{back} = vacuum vessel background temperature

The problem of emissivity taking part in eq. (2) is a major concern for IR temperature measurement but is a too wide scope to be treated in this study. Emissivity deals with many parameters as the surface state, the wavelength, the angle of incidence, and is more a concern of physics that is extensively treated in literature, recently in [7-10] regarding metallic fusion facility like WEST. Emissivity evaluation does not depend on the instrument quality nor calibration process. Thus it cannot be treated in the uncertainty calculation as the others parasitic sources. Since we only consider here the uncertainty from the instrument, we voluntarily not take into account the emissivity, which is equivalent to considering that $\epsilon_{obj}=1$ and then $Remit=R(T_{obj})$ is the black body radiance of the object. Equation (2) is not discuss anymore.

The knowledge of the transmission coefficient τ_i of each sub-system (measured in laboratory) and its temperature T_i (τ_i and T_i are discussed in §3) in operation on WEST allows the calculation of the object temperature by inverting eq. (1):

$$R(T_{obj}) = ((R_{mes} - (1-\tau_3).R(T_3))/\tau_3 - (1-\tau_2).R(T_2))/\tau_2 - (1-\tau_1).R(T_1))/\tau_1 \quad (3)$$

It remains to know the calibration curve of the camera to convert the Digital Level (DL) measured by the detector into radiance and then the final radiance $R(T_{obj})$, into blackbody temperature thanks to the Planks law.

Actually, this conversion is done afterwards. Eq. (3) is calculated in DL which are strictly proportional to the IR radiance, provided the camera detector is used in its linearity range, and the conversion from DL of the object to temperature is done directly using the calibration table $DL=f(T)$, i.e. without calculation of the physical radiance.

3 Uncertainties

3.1 calculation method

In equation (3), the same function (4) is propagated 3 times, for $i=3$ to 1:

$$R_i = (R_{i+1} - (1-\tau_i).R(T_i))/\tau_i \quad (4)$$

R_i radiance emitted from object side

R_{i+1} radiance at measurement side, transmitted through the optical sub-system i , at temperature T_i and transmission coeff. τ_i .

In particular: $R_4=R_{mes}$ and $R_1=Remit=R(T_{obj})$ in equations (1) and (2).

The error propagation of a function $f(x_i)$ is commonly given by the quadratic sum of its partial derivatives along the variables x_i that are assumed independent [11]: $(\Delta f)^2 = \sum_i \left(\frac{\delta f}{\delta x_i}\right)^2 \Delta x_i^2$ Δf and Δx_i being the standard or maximum deviations (see §3.2.1) of function f and variables x_i . Applied to (4) results in eq. (5):

$$\Delta R_i^2 = \left(\frac{\delta R_i}{\delta R_{i+1}}\right)^2 \Delta R_{i+1}^2 + \left(\frac{\delta R_i}{\delta R(T_i)}\right)^2 \Delta R(T_i)^2 + \left(\frac{\delta R_i}{\delta \tau_i}\right)^2 \Delta \tau_i^2 \quad (5)$$

Introducing function (4) in (5) lead to eq. (6):

$$\Delta R_i^2 = \left(\frac{1}{\tau_i}\right)^2 \Delta R_{i+1}^2 + \left(1 - \frac{1}{\tau_i}\right)^2 \Delta R(T_i)^2 + \left(\frac{R(T_i) - R_{i+1}}{\tau_i^2}\right)^2 \Delta \tau_i^2 \quad (6)$$

$\Delta R(T_i)$ = uncertainty of straylight due to the effect of temperature variation ΔT_i of each sub-system i

$$\Delta R(T_i) = (R(T_i + \Delta T_i) - R(T_i - \Delta T_i)) / 2 \quad (7)$$

$\Delta \tau_i$ = uncertainty of transmission coefficient

$\Delta R_4 = \Delta R_{mes}$ = uncertainty of the camera measurement

$\Delta R_{i=1 \text{ to } 3}$ comes from prior calculation iteration

Combining (4) and (6) in an iterative calculation with $i = 3$ to 1 gives at the end $\Delta R_1 = \Delta R(\text{Tobj})$ and then ΔTobj after conversion in temperature, which is the final overall uncertainty result.

Solving (6) necessitate the estimation of the specific uncertainties ΔR_{mes} ($=\Delta R_4$), $\Delta \tau_i$, ΔT_i , which is done in the next chapter.

3.2 Estimation of contributions to uncertainty

3.2.1 Standard or maximum deviation

The amount of data from the diagnostics is not sufficient to use eq. (6) with standard deviations values for the variables Δx_i . Thus, the specific uncertainties discussed here after (§3.2.2 to §3.2.4) are considered as the maximum values observed, and the overall uncertainty is directly given by ΔTobj .

3.2.2 Camera

The cameras are roughly composed of an InSb detector (SCD manufacturer) working in 1-5.5 μm wavelength band, an interferential filter @3.9 \pm 100 μm embedded in the camera just before the detector and thermalized at 14°C by Peltier effect, a magnetic shielding housing water cooled at 20°C, and a lens fixed to the housing. A multi-integration times mode is used to cover a large temperature range (typically 100-3000°C). The signal dynamic is coded on 13 bits that gives 8192 DL values, but the good linear range is limited to 6000 DL.

The uncertainty ΔR_{mes} of the IR camera measurement may come from:

- The detector response: the cameras detector features a linear response versus the collected radiance, for a given integration time (IT) (4 IT are used to cover the temperature range). Its sensitivity reproducibility is better than 0.1%, thanks to a very stable cooling of the focal plan array at 77K. A calibration test done after 2

years showed negligible differences. Therefore, uncertainty from detector is neglected.

- The filter bandwidth @3.9 \pm 100 μm . This band is accurately characterised by the manufacturer and results in insignificant uncertainty.

- The background: the camera background comprises the background radiance of the camera which acts as a parasitic radiance (similarly to the straylight), and the intrinsic noise of the detector. The latter is negligible compared to the background radiance. The filter, even if cooled at 14°C, is the dominant contributor to the background because it emits radiance in the entire detector band [1 - 5.5 μm] while its thin passband of 0.2 μm (4% of the band) well filters the rest of the background coming from optics and camera housing. At room temperature, the background mean value is roughly 2000 DL for the 1st IT (the largest one) and 800DL for the 4th IT (the shortest one). If it were constant, the background would have no effect on the uncertainty. However, its variations affect the accuracy. Laboratory tests disclosed that the background variation is about 60 DL for the largest integration time, due to the filter cooling variation ($\pm 0.2^\circ\text{C}$), and also to the camera housing temperature variation ($\pm 5^\circ\text{C}$) that affect the temperature filter itself, and that is the consequence of the fluctuation of the cold cooling loop and environment temperatures. The background level variation proportionally decreases with the integration time, but 10DL remains as a constant background noise.

- The camera lens: the camera lens transmission is integrated in the camera calibration (the camera is calibrated with its lens). Camera lens is cooled by conduction from the camera body; there is no measurable effect of the lens temperature variation on the camera background because the lens transmission is rather high (> 0.95).

- The detector Narcisse effect that can be observed under certain condition is known negligible.

3.2.3 Optical transmission

All optical parts impact the radiation propagation by reducing the radiated flus, and adding the parasitic straylight, as describe in §2.

The straylight uncertainty $\Delta R(T_i)$ due to optics temperature variation is calculated from eq. (7). The following values for temperature deviation ΔT_i are observed on WEST: 5°C for the components cooled by the cold loop at 20°C, 10°C for component at atmospheric temperature, and 30°C for parts cooled by the hoot loop (70°C). This last value is higher because it concern parts facing plasma or near parts facing plasma which can be somewhat heated by high heat flux.

The transmission coefficient uncertainty $\Delta \tau_i$ is mainly attributed to the non-homogeneity of the transmission in the optical field, and to the measurement procedure of τ_i (see §3.2.4). The minimum value between the followings is considered for $\Delta \tau_i$: a constant value of 0.03 or 10% of the transmission coefficient. An exception is made for the 1st mirror of antenna views which is close to the plasma (it is mounted on the inner wall of the vacuum vessel), and which can undergo

polluting deposits according to the experimental campaigns: a value of 0.15 is applied.

3.2.4 Calibration

Some uncertainty may come from the calibration process or from the test bed used for that. The calibration test bed allows the determination of the camera calibration curve, the correction of non-uniformity of the detector focal plan array, and the measurement of the optical transmission coefficients. The test bed essentially consists of reference devices (laboratory blackbodies) that are accurately calibrated by duty companies; their accuracy is inferior to 1%. Thus 1% is added by quadratic summation on the final temperature uncertainty ΔT_{obj} .

The camera calibration process is always done with the same procedure, and the same algorithm for linearization, which uses the Planck's law integral, whose calculation is considered exact. A linearization error of the sensor response of 1% is taken into account, even if it is quite better in reality, by applying coefficient 1.01 to ΔR_4 .

The optics transmission coefficient calibration is more prone to uncertainty, since it is hardly reproducible with accurateness due to some handling constraints. The resulting uncertainty gained from experience is given §3.2.3.

3.3 Uncertainty calculation result

3.3.1 Overall result

The Figure 3 shows the overall uncertainty calculated with the aforementioned method and data. The behaviour versus the temperature is similar for all views, despite important magnitude differences. One can observe a largest uncertainty at low temperatures for all diagnostics (see next chapter). After reaching a minimum, the uncertainty increases steadily with the temperature. Above 200°C, most uncertainties are much lower than 10%.

The antenna view is the worst-case due to a rather low overall transmission coefficient $\tau \approx 0.04$, which is the consequence of the use of numerous optics in a very compact optical design that was constrained by the tokamak integration. A low transmission coefficient drastically reduces the object radiance transmitted up to the camera compared to the parasitic disturbances.

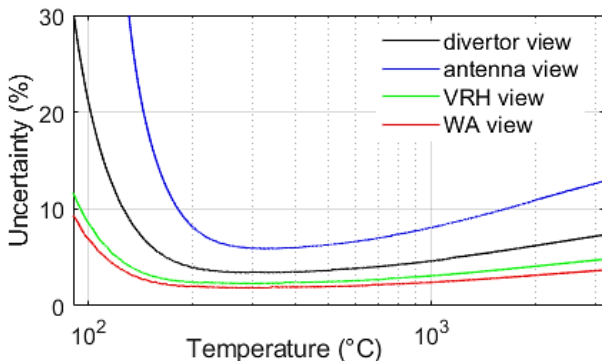


Figure 3 : overall uncertainty ΔT_{obj} calculated for the 4 kinds of WEST IR diagnostics

It is obvious that the zone where uncertainty is higher than 20% is not valuable and gives IR images blurred by the background. The temperature at 20% uncertainty roughly correspond to the minimum temperature detection that is usually observed (except for the VHR view, which is less sensitive due to its closed lens aperture $f/9$ instead of $\approx f/2$ for the others).

3.3.2 Focus on Divertor view

A detailed analysis of the influence of each specific uncertainty over the overall uncertainty is done on the divertor view (Figure 4). This view is chosen because it shows the average behaviour, but the analysis result is the same for all views. Table 2 summarizes the uncertainties values for divertor view used in the equation (6). These values comes either from laboratory or in-situ measurement.

Table 2: detailed uncertainties values for the divertor view.

Uncertainty contributor	Disturbance Values
1 st Optics Straylight	$\Delta T = \pm 30^\circ\text{C}$
1 st Optics transmission	$\Delta \tau = \pm 0.03$ with $\tau = 0.76$
2 nd Optic Straylight	$\Delta T = \pm 5^\circ\text{C}$
2 nd Optic transmission	$\pm 10\% * \tau$ with $\tau = 0.2$ $\Delta \tau = \pm 0.02$
Camera background	± 60 DL on ΔR_{mes} for 1 st IT, decreasing with IT
Camera linearity	$\pm 1\%$ on ΔR_{mes}
Test bed	$\pm 1\%$ on ΔT_{obj}

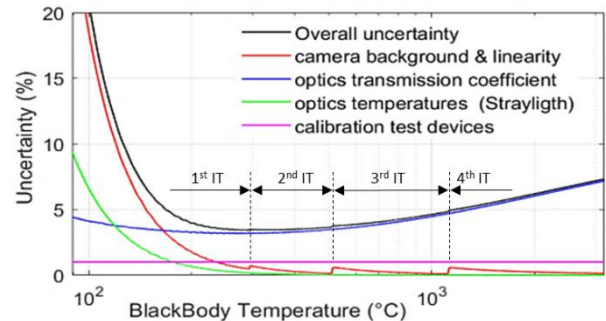


Figure 4 : contribution of each specific uncertainty to the overall one for the divertor views.

At low temperature, the camera uncertainty is the major contributor. Its effect is amplified by the low transmission coefficient in the case of divertor and antenna diagnostics. The temperature variation of the camera body and its filter, even if quite low, results in a variation of the camera background radiance that is detrimental for the low temperature measurement. This effect reappears more weakly when the integration time of the detector switches to the lower one (the cameras acquisition uses 4 integration times), when the radiance level have reached the maximum threshold. When the radiance increases for a given integration time, the camera background contribution tends to become negligible.

For high temperature, the transmission coefficient clearly dominates the uncertainty. The effect of optics temperature deviation is marginal compared to the rest; its trend decreases to 0%, as well as for the camera background.

The 1% uncertainty applied to ΔT_{obj} as contribution of the calibration devices contribution is a constant value almost negligible, due to the quadratic summation.

11. ROUAUD Mathieu. Calculs d'incertitudes
URL:<http://www.incertitudes.fr/Incertitudes.html>>

4 Conclusion

Due to the large number of parameters taking action in each IR diagnostic, this study may be considered as an approach of the temperature measurement uncertainty of WEST IR diagnostics. Moreover, one must keep in mind that the knowledge of material emissivity and the parasitic reflexions in metallic environment remain the main potential sources of error of quantitative IR measurement.

This study confirms and quantifies the following statements:

The low optical transmission is very unfavourable, specially highlighted on divertor and antenna views.

Camera thermalisation is a key point for low temperatures measurement. This point is taken into account on WEST with the use of a cooled filter, however it remains the main issue for temperature measurement accuracy. The use of steady cooling temperature controlled by the measurement of the camera internal temperature, at the same set point during calibration and operation, would reduce the uncertainty due to the camera background deviation. A filter integrated in the detector cryostat would also be an improvement, but this must be done at the camera design step, and then the filter features can never be changed afterward.

At low temperature, typically $<200^{\circ}\text{C}$, temperatures values should be use carefully, even if some rather good image quality can be observed at 150°C .

As for the rest of the temperature range, the instrument uncertainty is reasonable, which gives confidence in the temperature monitoring for the machine protection.

References

1. N. Fedorczak, et al., Nuclear Materials and Energy 27 (2021) 100961
2. X. Courtois, et al., Fusion Eng. Des. 136 B (2018) p1499–1504.
3. X. Courtois, et al., Fusion Eng. Des. 146 (2019) p2015-2020
4. M. Houry, et al., Fusion Eng. Des. – to be published (32nd SOFT proceedings)
5. M. Houry, et al., Fusion Eng. Des. 146 A (2019) p1104-1107,
6. C. Desgranges, et al., Nuclear. Ints. & Methods in Physics Research, A, 879 (2018), p121-133
7. M-H. Aumeunier, et al., Nuclear Materials and Energy, 26 (2021) 100879
8. J. Gaspar et al., Fusion Eng. Des. 149 (2019), 111328
9. D. Guilhem, et al., Nucl. Fusion 61 (2021) 096003
10. J. Gaspar et al., Nucl. Fusion (2022) 0029-5515